



Proton implantation and rapid thermal annealing effects on GaAs/AlGaAs quantum well infrared photodetectors

NA LI, NING LI, W. LU, X. Q. LIU, X. Z. YUAN, Z. F. LI, H. F. DOU, S. C. SHEN

National Laboratory for Infrared Physics, Shanghai Institute of Technical Physics, Chinese Academy of Sciences, 500 Yu Tian Road, Shanghai 200083, People's Republic of China

Y. FU, M. WILLANDER

Microelectronics Center at Chalmers, Physical Electronics and Photonics, Department of Physics, Chalmers University of Technology and University of Gothenburg, Fysikgränd 3, S-41296 Gothenburg, Sweden

L. FU, H. H. TAN, C. JAGADISH

Department of Electronic Materials Engineering, The Research School of Physical Sciences and Engineering, The Australian National University, Canberra ACT 0200, Australia

M. B. JOHNSTON, M. GAL

School of Physics, The University of New South Wales, Sydney NSW 2052, Australia

(Received 5 August 1999)

We report the use of intermixing techniques to modify GaAs/AlGaAs multiple quantum wells (MQWs). A large shift in the response wavelength of the GaAs/AlGaAs MQW-based infrared photodetector is obtained by proton implantation and then a standard annealing procedure (950 °C for 30 s). The photoluminescence (PL) and photoresponse spectra were measured as functions of ion dose in the range from 5×10^{14} to $2.5 \times 10^{15} \text{ cm}^{-3}$. The peak photoresponse wavelength was tunable between 8.2 and 9.8 μm for the infrared radiation and the energy position of the PL peak from the MQW material changed from 1.62 to 1.645 eV. The effects of the ion implantation and thermal annealing on the device performance have been well characterized theoretically by the inter-diffusion of Al atoms across the GaAs/AlGaAs heterointerfaces and the relaxation energy of free carriers.

© 1999 Academic Press

Key words: GaAs/AlGaAs, quantum well, infrared photodetector, Al intermixing, ion implantation.

1. Introduction

There has been rapid progress in quantum well (QW) infrared photodetectors (QWIPs) based on matured QW III–V materials and device processing technologies [1, 2]. The linear array [3] and focal plane array (FPA) [4] investigations have demonstrated the excellent QWIP capability of accessibly large area FPAs

for long wavelength infrared and multiple-color applications [5]. Further research activities on intersub-band physics, detector performance and optimization accelerate greatly the development of practical QWIP devices. Recently, researchers have been interested in the application of quantum well intermixing (QWI) techniques [6, 7] to modify energy levels of GaAs/AlGaAs multiple quantum wells. QWI has drawn considerable interest because of its wide applicability in optoelectronics, as it can easily modify the geometric shape of the quantum well to allow postgrowth adjustments of key physical parameters such as effective bandgap, optical absorption coefficient and refractive index. Selective QWI and thus selective modification of epitaxial structures are necessary for the fabrication of novel optoelectronic devices integrated into a single microchip. A number of methods have been developed to modify the optical and electrical characteristics of quantum well structures including ion-implantation-induced intermixing, anodic-oxidation-induced intermixing [8] and SiO₂ capping [9] followed by rapid thermal annealing (RTA).

The ion-implantation-using materials such as Si [10] and As [11] and then further encapsulation by a dielectric layer such as SiO₂ and Si₃N₄ have been proven to be rather effective in enhancing the QWI selectively. Ion implantation allows various defects to be introduced into a semiconductor with high precision control in a three-dimensional manner. The two-dimensional surface structure is obtained by the standard mask technique and the depth of the defect distribution in the semiconductor can be controlled by adjusting the kinetic energy and/or the mass of the ions. In this work we demonstrate, both experimentally and theoretically, that the proton implantation can largely modify the material characteristics and device performance after standard annealing procedures. The experiments are described in Section 2 and the measurement spectra and theoretical analysis are presented in Section 3 followed by a brief summary.

2. Experiment setups

The GaAs/AlGaAs multiple quantum well (MQW) materials used for our QWI study were grown by molecular beam epitaxy on a semi-insulating GaAs substrate. It consists of 50 periods of 4.6 nm Si-doped ($5 \times 10^{17} \text{ cm}^{-3}$) GaAs wells separated by 50 nm undoped Al_{0.3}Ga_{0.7}As barriers. This MQW structure is sandwiched between two GaAs contact layers (each 1 μm and Si-doped to a level of $2 \times 10^{18} \text{ cm}^{-3}$).

The ion implanter used in this study was a 1.7 MeV tandem. The protons were originated from TiH powder pressed into a Cu electrode. Aluminium was used to mask the regions of the sample to be implanted. Proton implantation was performed at energies from 300 to 420 KeV. Multiple energy implantation was used (implantation with ions with single energy produce a narrow damage profile as a function of spatial depth). The multiple energy implantation steps were designed to create homogeneous QWI across the 50 quantum wells (covering a depth in the sample of 2.7 μm), and hence a reliable tuning, rather than a broadening of the QWIP infrared spectral response. The density of proton implantation ranges from 5×10^{14} to $2.5 \times 10^{15} \text{ cm}^{-3}$.

After implantation, all samples were annealed at 950 °C for 30 s in a flowing nitrogen environment within a rapid thermal anneal (RTA) apparatus, with the samples covered by a clean piece of GaAs material to reduce surface degradation due to As out-diffusion. An array of $250 \times 250 \mu\text{m}^2$ mesas (QWIP) were then fabricated by wet etching through the upper contact and MQW structure, followed by the deposition and alloying of AuGeNi/Au contacts.

3. Experimental results and theoretical analysis

Qualitatively, it is expected that due to the ion implantation and annealing, the Al atoms diffuse from barrier regions into well regions. The abrupt GaAs/AlGaAs heterointerfaces become destroyed. The bottom of the quantum well is lifted up and the width of the quantum well is effectively reduced. The subband energies of carriers (electron/hole) are thus increased with respect to the GaAs bandedges (conduction/valence bandedges).

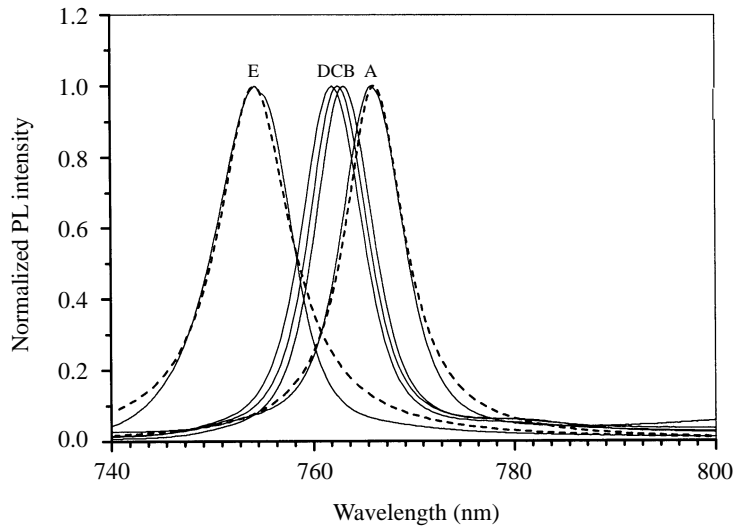


Fig. 1. Photoluminescence (PL) measurements at 77 K. The dashed lines were obtained theoretically. Curve: A, as grown; B, anneal 950°C, 30 s; C, $5 \times 10^{14} \text{ cm}^{-3} \text{ H}^+$; D, $1 \times 10^{15} \text{ cm}^{-3} \text{ H}^+$; and E, $2.5 \times 10^{15} \text{ cm}^{-3} \text{ H}^+$.

Photoluminescence (PL) measurements at 77 K were performed on all of the samples, which were implanted with different doses and then annealed. A blueshift of the PL peak is observed in the Fig. 1, from 766 nm (as-grown sample) to 754 nm (sample with protons implanted to $2.5 \times 10^{15} \text{ cm}^{-3}$). As discussed in the last paragraph, due to the Al atomic diffusion, subbands of conduction-band electrons and valence-band holes move further apart, causing an increase in the transition energy between electron and heavy hole subbands, and thus a blueshift of the excitonic energy as observed in the PL spectra.

The chip containing detector elements was packaged in a standard QWIP test geometry with a 45° polished facet for optical coupling. The photocurrent spectra of QWIP were measured in a Fourier transform spectrometer at 77 K. The detector was back illuminated at 80 K and mounted in a liquid-nitrogen-cooled cold finger Dewar.

The dark current–voltage curves on mesa devices are shown in Fig. 2A. The bias voltage on devices is negative ranging from zero to -9 V . Note that the dark current increases by nearly a factor of 2 after proton implantation while it is almost unchanged after the annealing processes.

Figure 3A shows the photocurrent spectra at a negative bias of about -3 V . Peak response wavelengths are 8.17, 8.58 and $9.85 \mu\text{m}$ for sample A (as grown), sample D (proton implantation dose $1 \times 10^{15} \text{ cm}^{-3}$) and sample E ($2.5 \times 10^{15} \text{ cm}^{-3}$), respectively. Significant redshifts of peak response wavelength were observed in the proton implanted samples (maximally $1.7 \mu\text{m}$ shift for sample E). The result is expected qualitatively as the separation from the discrete state to the continuum states above the barrier is reduced.

Quantitatively, we define the quantum well growth direction as the z -axis. The quantum well is changed from a square well, with rather sharp heterointerfaces, to an error-function-shaped well. The degree of the Al diffusion is given by Fick's diffusion equation [12–14]

$$x(z) = x_0 \left\{ 1 + \frac{1}{2} \left[\operatorname{erf} \left(\frac{z - W/2}{2L} \right) - \operatorname{erf} \left(\frac{z + W/2}{2L} \right) \right] \right\}, \quad (1)$$

where x_0 is the initial Al mole fraction in the barrier, W the quantum well width, L the diffusion length, and erf the error function. The center of the well is taken as $z = 0$.

We start the theoretical analysis in the usual way by the self-consistent calculation of Schrödinger and

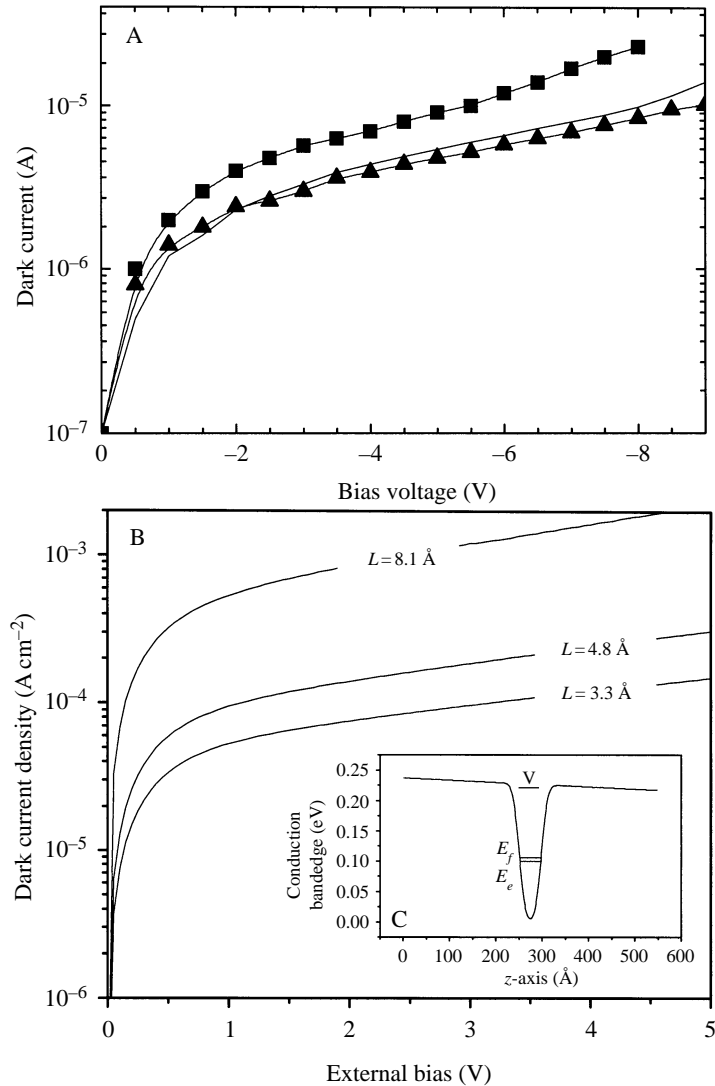


Fig. 2. A, Dark current: —, as grown; —▲—, anneal; —■—, $2.5 \times 10^{15} \text{ cm}^{-3} \text{ H}^+$. B, Calculated dark current densities for different QWI conditions. C, Energy band structure with 1.0 V external bias.

Poisson equations to obtain the energy band structure and carrier distribution of our multiple GaAs/AlGaAs multiple quantum well system. Quasi-Fermi levels of 86 meV above the GaAs conduction band edge are obtained at 77 K in the emitter and collector doped to $2 \times 10^{18} \text{ cm}^{-3}$. The ground sublevel E_0 in the quantum well is 82 meV and the quasi-Fermi level there is 9.2 meV above E_0 when the central 3 nm layer of the quantum well is doped to 10^{18} cm^{-3} . A flat band situation is then expected. This numerically confirms that the electric Coulomb potential due to the doped donors and the free charge redistributions in well regions is negligibly small. The conclusion is due to the low doping level in the quantum well and the almost coincident spatial distributions of donors and free carriers at the ground sublevel of the quantum well. We thus observe an almost linear distribution of the external bias across the MQW system.

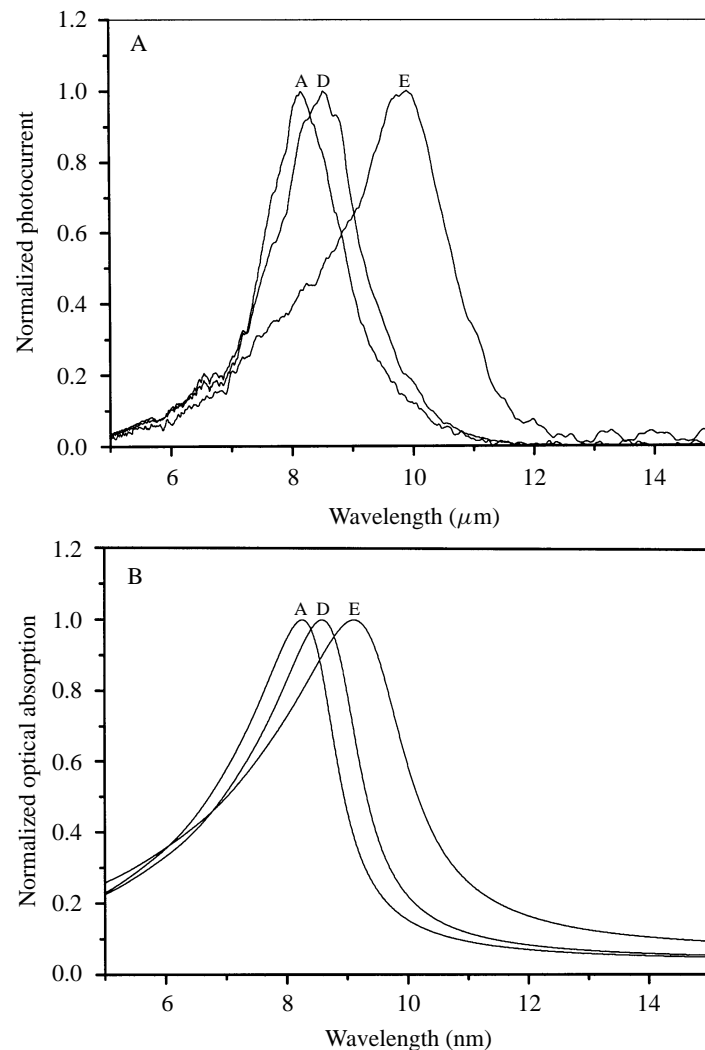


Fig. 3. Photocurrent spectra of QWIP were measured in a Fourier transform spectrometer at 77 K. Curve: A, as grown, 8.17 μm ; D, $1 \times 10^{15} \text{ cm}^{-3} \text{ H}^+$, 8.58 μm ; and E, $2.5 \times 10^{15} \text{ cm}^{-3} \text{ H}^+$, 9.85 μm .

We first study the PL spectrum of the system when the external bias is zero. At low temperature the excitonic effect is very important. By a three-dimensional hydrogenic-type wavefunction, the ground state binding energy E_b of an exciton consisting of a valence-band heavy hole and a conduction-band electron is calculated and a binding energy of $E_b = 10.6 \text{ meV}$ is obtained [16]. Experimentally, the PL peak from the GaAs substrate was located at 820 nm at 77 K, indicating an energy bandgap of the substrate GaAs as 1.519 eV [15] when the bulk exciton binding energy in the GaAs material is included.

Due to the nature of the growth kinetics and mechanisms, the diffusion of Al atoms from the AlGaAs layer to the GaAs layer is inevitable, resulting in a \pm monolayer fluctuation during the thin film growth process. This monolayer fluctuation has been reflected by the PL peak position shift in the narrow well structure. A thickness change due to a one-monolayer fluctuation in a [001] GaAs/AsGaAs heterointerface corresponds to a diffusion length of 2.8 \AA . However, the fitted PL spectrum indicates a diffusion length of $L = 3.3 \text{ \AA}$

and the calculated transition energy is 765.9 nm (curve A, as grown, $\Gamma = 7.5$ meV is the carrier relaxation energy to be discussed).

When considering electron and hole recombination (photoluminescence), the transition probability per unit time for the emission of a light quantum $\hbar\omega$ is [17]

$$W = \frac{\Gamma\omega}{(E_e - E_h - \hbar\omega)^2 + \Gamma^2} \left| \left\langle \phi_e \left| \frac{\partial}{\partial z} \right| \phi_h \right\rangle \langle u_c | u_v \rangle + \langle \phi_e | \phi_h \rangle \left\langle u_c \left| \frac{\partial}{\partial z} \right| u_v \right\rangle \right|^2 \quad (2)$$

apart from physical constants. (E_e, ϕ_e) and (E_h, ϕ_h) are eigenstates of conduction-band electron and valence-band heavy hole, u_c and u_v are Bloch functions of conduction and valence bands. Γ is the effective relaxation energy of carriers. Here, due to the low doping level in the quantum well and low temperature, only the ground electronic sublevel is occupied so that we only need to consider the ground sublevels of the conduction-band electron and valence-band heavy hole. Because of the unknown parameters of $\langle u_c | u_v \rangle$ and $\langle u_c | \partial u_v / \partial z \rangle$, we calculated $\langle \phi_e | \partial \phi_h / \partial z \rangle$ and $\langle \phi_e | \phi_h \rangle$ separately. However, since we consider only the ground sublevels, the PL spectrum is determined by $\Gamma\omega / [(E_e - E_h - \hbar\omega)^2 + \Gamma^2]$. By matching the calculated PL spectra with the corresponding measurements (solid lines in Fig. 1) we have easily obtained the diffusion length and relaxation energy: 4.8 Å, 7.5 meV, (curve B: 763.5 nm); 5.1 Å (curve C: 763.1 nm); 5.4 Å (curve D: 762.1 nm); and 8.1 Å, 9.5 meV, (curve E: 754.3 nm).

It is observed here that the ion implantation increases the Al diffusion length as well as the carrier relaxation energy (reduced carrier lifetime), as can be expected qualitatively.

We now calculate the dark currents under various QWI conditions. The dark current is defined as the sum of the tunneling current transmitting below the barrier height and the thermoexcited drift-diffusion current transmitting above the barrier height. It is known numerically that the occupation of the states below the barrier height is high while the transmitting amplitude is rather low due to the large barrier width. The effective transmitting amplitude is close to one when the electron energies are above the barrier height. However, the corresponding occupation of these states is very low. Numerically, we have found here that in our system, the thermoexcitation dominates while the direct tunneling process is several orders lower due to the rather thick barrier width.

By assuming quasi-equilibrium states in the contact layers and in every quantum well, it is found that the self-consistently calculated electric field in each quantum barrier region is almost constant (low free carrier concentration and thus high resistivity), while the one in the quantum well region is almost zero (high free carrier concentration and thus low resistivity). It is also obtained that the accumulation and depletion layers in the contact layers are negligibly thin as compared with the MQW thickness. The thermally activated current density has been modeled as [18–21]

$$J = evn, \quad (3)$$

where v is the carrier drift velocity given by

$$v = \mu F \left[1 + \left(\frac{\mu F}{v_s} \right)^2 \right]^{-1/2}, \quad (4)$$

v_s is the saturation drift velocity of about 5×10^6 cm s⁻¹, μ is the low field carrier mobility having a value of 2000 cm² (volt · s)⁻¹ for n-type AlGaAs QWIPs, and F is the electric field intensity in the MQW. The density of mobile carriers n is computed as

$$n = \frac{1}{L_{\text{MQW}}} \sum_i \int \frac{2dk}{(2\pi)^2} |t(E_i, E_k)|^2 f(E_i, E_k), \quad (5)$$

where L_{MQW} is the period of the MQW (the sum of quantum well width and barrier width), i is the index of energy subband E_i in the quantum well region (it includes both the discrete energy sublevels as well as

the continuum states above the barrier), \mathbf{k} is the wavevector in the xy -plane. $f(E_i, E_k)$ is the Fermi–Dirac distribution function.

$$t(E_i, E_k) = \begin{cases} 1, & \text{if } E_i + E_k > V, \\ 0, & \text{otherwise} \end{cases} \quad (6)$$

when only considering the thermal excitation. Here, V is the barrier height at the right-hand side of the quantum well when the sample is biased (see Fig. 2C). With the diffusion length and relaxation energy obtained from the PL spectra, the calculated dark current densities are presented in Fig. 2B which agree very well with the measurement results.

Corresponding to the measured photocurrent spectra in Fig. 3A, the calculated optical absorption coefficient is presented in Fig. 3B. As in the normal situation, the electron–photon interaction is perturbative so that the carrier redistribution due to the photoexcitation is hardly important enough to cause extra Coulomb potential. The photocurrent is proportional to the density of photocarrier, which in its turn is proportional to the optical absorption coefficient. (The proportional constant between photocurrent and photocarrier, i.e. the drift velocity, is constant at the same external bias when measuring photocurrent.)

With the diffusion length and relaxation energy obtained from the PL spectra, the calculated wavelengths at the peak absorption are 8.26 (sample A), 8.58 (sample D) and 9.11 μm (sample E). General agreements between measurement and calculation are observed. However, discrepancies cannot be neglected. The difference between the shapes of the absorption coefficient peak and the corresponding photocurrent indicates a different value of relaxation energy as compared with the PL spectrum. It is due to the different physical processes (electron–hole recombination with respect to transitions from discrete sublevels to continuum states). The difference in the observed and calculated redshifts, however, demands a more sophisticated theoretical model to calculate the photocurrent. Two most important physical factors are the electric field effect in the calculation of the absorption coefficient and then the processes of relaxing energies of carriers gained from the electric field during the transport from the emitter to the collector.

In this brief summary it is concluded that, by the consistent comparisons between measurements and theories (PL spectra of the material, dark current, photocurrent and optical absorption coefficients of QWIP devices), the quantum well intermixing effect induced by ion implantation and rapid thermal annealing is very significant. The energy sublevel is lifted up with respect to the corresponding carrier's bandedge and the peak detection wavelength of an operational quantum well infrared photodetector has red shifted by proton ion implantation and rapid thermal annealing processes.

Acknowledgement—Financial support from the Australian Agency for International Development (AusAID) through IDP Education Australia under Australia–China Institutional Links Program is acknowledged.

References

- [1] B. F. Levine, *J. Appl. Phys.* **74**, R1 (1993).
- [2] K. K. Choi, *The Physics of Quantum Well Infrared Photodetector* (World Scientific, Singapore, 1997).
- [3] M. F. Wan, H. J. Ou, and W. Lu, *J. Infrared Millim. Waves* **17**, 76 (1998).
- [4] S. D. Gunapala *et al.*, *IEEE Trans. Electron Devices* **44**, 51 (1997).
- [5] H. C. Liu, J. Li, and J. R. Thompson, *IEEE Trans. Electron Devices* **14**, 566 (1993).
- [6] B. Elman, E. S. Koteles, P. Melman, and C. A. Armiento, *J. Appl. Phys.* **66**, 2104 (1989).
- [7] H. H. Tan, J. S. Williams, C. Jagadish, P. T. Burke, and M. Gal, *Appl. Phys. Lett.* **68**, 2401 (1996).
- [8] S. Yuan, Y. Kim, C. Jagadish, P. T. Burke, and M. Gal, *Appl. Phys. Lett.* **83**, 1305 (1998).
- [9] J. Y. Chi, X. Wen, E. S. Koteles, and B. Elman, *Appl. Phys. Lett.* **55**, 855 (1989).
- [10] P. Gavrilovic, D. G. Depoe, K. Meehan, and N. Holonyak, *Appl. Phys. Lett.* **47**, 130 (1985).
- [11] A. G. Steele, M. Buchanan, H. C. Liu, and Z. R. Wasilewski, *J. Appl. Phys.* **75**, 8234 (1994).

- [12] G. F. Redinbo, H. G. Craighead, and J. M. Hong, Proton implantation intermixing of GaAs/AlGaAs quantum wells, *J. Appl. Phys.* **74**, 3099 (1993).
- [13] W. Feng, F. Chen, W. Q. Cheng, Q. Huang, and J. M. Zhou, Influence of growth conditions on Al-Ga interdiffusion in low-temperature grown AlGaAs/GaAs multiple quantum wells, *Appl. Phys. Lett.* **71**, 1676 (1997).
- [14] J. Crank, *The Mathematics of Diffusion* (Clarendon, Oxford, 1956).
- [15] *Semiconductors: Group IV Elements and III-V Compounds*, edited by O. Madelung (Springer-Verlag, Berlin, 1991) p. 101.
- [16] Y. Fu and K. A. Chao, Exciton binding energy in GaAs/AlGaAs multiple quantum wells, *Phys. Rev.* **B43**, 12626 (1991).
- [17] Y. Fu and M. Willander, *Physical Models of Semiconductor Quantum Devices* (Kluwer, Boston, MA, 1999) p. 181.
- [18] S. R. Andrews and B. A. Miller, Experimental and theoretical studies of the performance of quantum well infrared photodetectors, *J. Appl. Phys.* **70**, 993 (1991).
- [19] R. L. Whitney, K. F. Cuff, and F. W. Adams, Long wavelength infrared photodetectors based on inter-subband transitions in III-V semiconductor quantum wells, in *Semiconductor Quantum Wells and Superlattices for Long-wavelength Infrared Detectors*, edited by M. O. Manasreh (Artech House, Boston, MA, 1993), Chap. 3, pp. 55–108.
- [20] B. F. Levine, C. G. Bethea, G. Hasnain, V. O. Shen, E. Pelve, R. R. Abbott, and S. J. Hsieh, High sensitivity low dark current 10 μm GaAs quantum well infrared photodetector, *Appl. Phys. Lett.* **56**, 851 (1990).
- [21] G. M. Williams, R. E. DeWames, C. W. Farley, and R. J. Anderson, Excess tunnel currents in Al-GaAs/GaAs multiple quantum well infrared detectors, *Appl. Phys. Lett.* **60**, 1324 (1992).